

Measurement of the high energy γ -rays from heavy ion reactions using Čerenkov detector

Dawei Si^a, Yan Zhou^a, Sheng Xiao^a, Zhigang Xiao^a

^a*Department of Physics, Tsinghua University, Beijing 100084, China*

Abstract

The energetic bremsstrahlung photons up to 100 MeV produced in heavy ion collisions can be used as a sensitive probe to the short range correlation in atomic nuclei. The energy of the γ -rays can be measured by collecting the Čerenkov light in medium induced by the fast electrons generated in Compton scattering or electromagnetic shower of the incident γ ray. Two types of detectors, based on pure water and lead glass as the sensitive material respectively, are designed for the above purpose. The γ response and optical photon propagation in detectors have been simulated based on the electromagnetic and optical processes in Geant4. The inherent energy resolution of $0.022 + 0.51/E_\gamma^{1/2}$ for water and $0.002 + 0.45/E_\gamma^{1/2}$ for lead glass are obtained. The geometry size of lead glass and water are optimized at $30 \times 30 \times 30 \text{ cm}^3$ and $60 \times 60 \times 120 \text{ cm}^3$, respectively, for detecting high energy γ -rays at 160 MeV. Hough transform method has been applied to reconstruct the direction of the incident γ -rays, giving the ability to distinguish experimentally the high-energy γ rays produced in the reactions on the target from the random background cosmic ray muons.

1. Introduction

Bremsstrahlung high-energy photons produced in heavy ion reactions has attracted increasing interest for its relevance to the nuclear equation of state (nEOS) and to the short range correlation in nuclei. For the studies of nEOS, particularly for the nuclear matter with large neutron-to-proton asymmetry, a variety of isospin probes have been identified to constrain $E_{\text{sys}}(\rho)$ (the density dependent nuclear symmetry energy), including preequilibrium n/p yield ratio[1], n/p differential flow[2, 3] and the Bremsstrahlung high-energy photons [4] etc. Among these probes, Bremsstrahlung γ -rays created in heavy ion collisions is a clean observable because of its rare interactions with the medium after it is produced. Very recently, it has been pointed out that the Bremsstrahlung high-energy γ carries the information of the high momentum tail (HMT) of nucleons, giving rise to the short range correlation effect in nuclei[5, 6, 7, 8]. On the other hand, however, the experimental data on this direction is quite scarce.

Recently, the full γ energy spectrum up to 80 MeV has been measured in the reactions $^{86}\text{Kr}+^{124}\text{Sn}$ at 25 MeV/u with a 15-unit CsI(Tl) hodoscope mounted on the compact spectrometer for heavy ion experiment (CSHINE)[9, 10, 11, 12]. It has been demonstrated that the γ energy spectrum above 20 MeV is reproduced fairly well by the transport model simulations incorporating the γ production from the incoherent np scattering with approximate 15% HMT ratio [13]. However, CsI(Tl) is a slow detector, the microsecond response time of CsI(Tl) crystals makes it complicated to reconstruct the total energy from multiple firing units. Therefore, it is our motivation to develop a fast and relative cheap detector containing sufficiently large-volume sensitive material to detect the high energy γ -rays in

heavy ion reactions. The Čerenkov radiation detector is a favorable option because of its fast response time in the order of tens nanoseconds and its ability to infer the incident direction information of the initial γ -rays, the latter of which can be used to suppress the cosmic-ray muon background from random directions.

In this paper, we report the design of a Čerenkov γ calorimeter using water and lead glass, respectively, as sensitive medium. Based on Geant 4 packages, the geometry size of the detectors is optimized. The energy resolution is obtained by tracking each Čerenkov photon before they arrive at the photomultiplier tube (PMT), of which the quantum response is modeled. The incident direction reconstruction is implemented by Hough transform method. The paper is organized as following. Section 2 presents the simulations framework of the calorimeter. Section 3 presents the optimization of detector size and the reconstruction of γ direction. Section 4 is the conclusion.

2. Simulation Setup

In this study, Geant4 (version 4.10.05)[14] packages are used for Monte Carlo simulation and optimization of the detector. “QBBC” and “G4OpticalPhysics” are applied as the physical process list to describe the electromagnetic (EM) showers of γ rays in materials, and to model the generation and transport of Čerenkov photons. For each event in the simulations, the incident γ -ray hits the front of the detector. Then the Čerenkov photons are generated if fast electrons are produced by Compton scattering or by e^-e^+ generation. Each Čerenkov photon is tracked to its termination, either to be absorbed in propagation or to reach the surface of the PMTs, where the waveform pulse of given parameters is generated with a certain quantum efficiency. The waveform is recorded at an interval of 2 ns for digitization. The final data corresponding to each incident γ

Email address: xiaozg@tsinghua.edu.cn (Zhigang Xiao)

ray is saved as a matrix of $N_1 \times N_2$ dimensions, where N_1 represents the number of fired PMTs and N_2 represents the number of sampling points for the corresponding waveform.

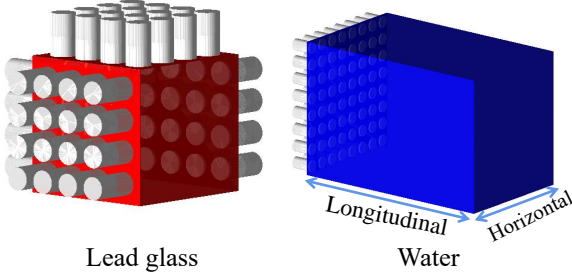


Figure 1: (Color online) Detector configuration with two sensitive volumes, lead glass (left) and pure water (right), respectively.

2.1. Detector geometry

The detector structure and the locations of the PMTs are shown in Fig.1 for lead glass and water as sensitive material, defined by "G4_GLASS_LEAD"(left) and "G4_WATER"(right), respectively. The water tank size is $60 \times 60 \times 120 \text{ cm}^3$, and the lead glass is $30 \times 30 \times 30 \text{ cm}^3$. The PMTs are arranged in an 8×8 array in water configuration. For lead glass configuration, PMTs are placed as 4×4 arrays on four sides of the detecting tank. The diameter of the PMT was 51 mm, and the distance between each neighboring PMT pair is 70 mm both vertically and horizontally.

2.2. Optical process

After invoking the Čerenkov mechanism in Geant4, the energy and number of Čerenkov photons are sampled in each G4step according[15].

$$\frac{d^2 N}{d\lambda dL} = \frac{2\pi\alpha Z^2}{\lambda^2} \sin^2 \theta_c \quad (1)$$

where θ_c is the Čerenkov angle, λ is the wavelength of Čerenkov photon. The initial position of Čerenkov photons is uniformly distributed in every G4step, the emission angle is calculated according to the refractive index of materials and the speed of charged particle, the outgoing azimuth is uniformly distributed within the range of 2π , we set a maximum of 100 photons emitted in each step to ensure the detailed sampling. In the process of photon transport, the transmission characteristics of photons in the material and the behavior at the boundary between two materials need to be defined. In this simulation, we defined the scattering and absorption lengths between Čerenkov photons and water molecules by referring to the test data of IceCube[16, 17]. Due to the lack of optical parameters of lead glass, we conservatively defined the attenuation efficiency of 70% for 10 cm propagation. For the boundary characteristics[18, 19], we used

UNIFIED model[20, 21] in Geant4 and selected "dielectric-dielectric" option to describe the interface between the material and PMTs. In this model, Geant4 will determine the photon boundary behavior according to Fresnel formula and refractive index on both sides. At the remaining boundaries, we used the dielectric.LUT model[22] and selected the polished Teflon.LUT boundary. In this way, Geant4 will determine the reflection, refraction and absorption of photons based on built-in parameters.

2.3. PMT Response

In the full situations, photons will be converted into photoelectrons with a certain quantum efficiency after hitting PMT, and pulse will be formed after multiplication. The pulse formed by a single photon is described by [23]

$$V_{\text{pulse}}(t) = \begin{cases} G \exp(-\frac{1}{2}(\frac{t-t_i}{\sigma} + e^{\frac{t-t_i}{\sigma}})), & t \leq t_i \\ G \exp(-\frac{1}{2}(\frac{t-t_i}{\sigma})^{0.85} + e^{\frac{t-t_i}{\sigma}}), & t > t_i \end{cases} \quad (2)$$

where $t_i = t_{\text{hit}} + t_{\text{trans}}$, t_{hit} represents the time when a photon hits PMT, $t_{\text{trans}} = 29 \text{ ns}$ represents the electron transit time of PMT, $\sigma = 1.2 \text{ ns}$ is the transit time spread. When multiple photons were converted into photonelectrons, the final waveform is generated by superimposing all single-photon waveforms as Fig.2(a) shown. Counting from the incidence of the γ ray, the waveform of each PMT within 240 ns was recorded as the final data. Fig.2(b) shows the distribution of the time when optical photons reach on PMTs in lead glass configuration which was extracted by linear fitting the rising edge of waveform[24]. It illustrates most photons reach on the surface of PMTs between 26ns and 31ns after the γ emission, which means we can distinguish between direct and scattered photons according to the distribution in the direction reconstruction (see section 3).

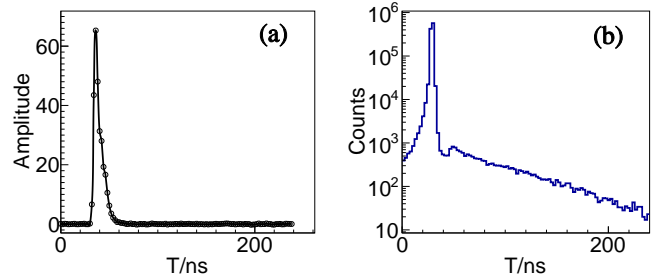


Figure 2: (Color online) (a) a typical waveform for PMT, (b) the distribution of the time when optical photons reach on PMTs in lead glass detector.

3. Result and discussion

3.1. Influence of detector size on energy resolution

We use the the photoelectron peak number $\langle n_{\text{pe}} \rangle$ and the energy resolution, defined by $\delta_{E_\gamma} = \delta_{n_{\text{pe}}} = \sigma_{n_{\text{pe}}} / \langle n_{\text{pe}} \rangle$, to optimize the detector design. In the simulation, such high-energy γ rays hit perpendicularly the center of the front surface of detector. The shower electrons and positrons, if produced with velocity exceeding the speed of light in the medium, will generate

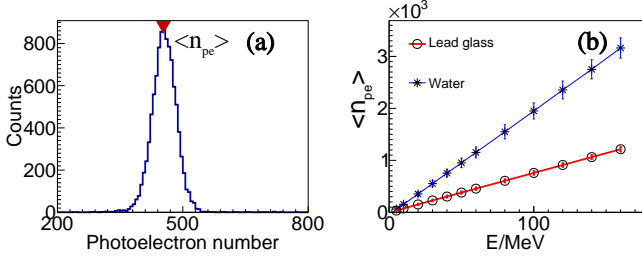


Figure 3: (Color online) (a) the spectrum of the photoelectron yield for 50 MeV γ rays in lead glass detector, (b) Linear response of the calorimeter.

\checkmark Čerenkov light propagating to the PMT where the photoelectrons are generated. Due to statistic fluctuations, the number of photoelectrons varies. Fig. 3 (a) presents the distribution of the number of photoelectrons for 50 MeV incident γ ray in the lead glass detector as an example. The photoelectron peak number $\langle n_{pe} \rangle$ is taken as the average number of photoelectrons in the following analysis. Fig. 3 (b) presents the distribution of $\langle n_{pe} \rangle$ as a function of incident γ energy E_γ for the two configurations at their own optimized volume (see below). It is shown that for either detector with given size, $\langle n_{pe} \rangle$ exhibits a linear dependence on E_γ . Thus, the γ ray energy can be measured by the number of photoelectrons.

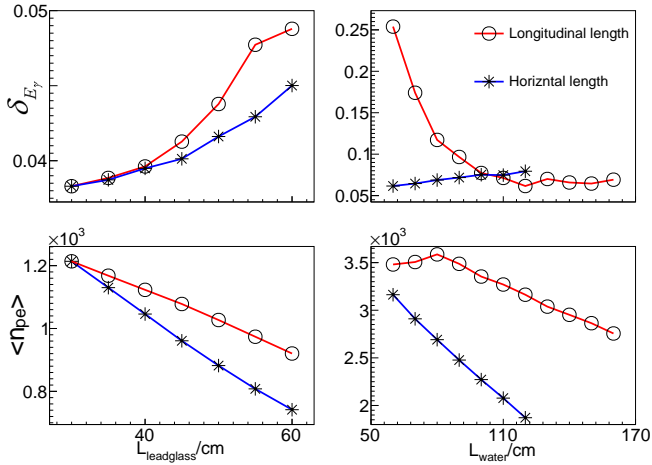


Figure 4: (Color online) process of size optimization. (a) relationship between energy resolution and detector size for lead glass, (b) relationship between energy resolution and detector size for water, (c) relationship between $\langle n_{pe} \rangle$ and detector size for lead glass, (d) relationship between $\langle n_{pe} \rangle$ and detector size for water.

We then optimize the detector size at a given maximum γ energy of 160 MeV, which covers the range of interest of E_γ in the heavy ion reactions at Fermi energies. In each event the distribution of photoelectron number is analyzed to obtain the $\langle n_{pe} \rangle$ and the standard deviation ($\sigma_{n_{pe}}$) of the distribution. If the size of the detector medium is too small, much of the γ ray energy will leak to outside of the sensitive volume. On the other hand, if the detector medium is too large, Čerenkov photon will be scattered many times and gradually absorbed, leading to the reduction of photoelectron number collected by PMTs. These

two factors compete with each other and determines the energy resolution. Fig.4(a) and (c) illustrate the energy resolution δ_{E_γ} and $\langle n_{pe} \rangle$ as a function of the horizontal and longitudinal length for the lead glass configuration. Clearly, as the horizontal and longitudinal length increases, δ_{E_γ} increases, while $\langle n_{pe} \rangle$ decreases, respectively. So $30 \times 30 \times 30 \text{ cm}^3$ is the optimal size for lead glass. Fig.4(b)(d) shows the same quantities in pure water configuration. With increasing the longitudinal length, the energy resolution δ_{E_γ} decreases gradually and converges to 6%, and $\langle n_{pe} \rangle$ first increases and then decreases, because Čerenkov light attenuation becomes the main factor after the longitudinal length exceeds 80cm. As horizontal length increases, δ_{E_γ} increases and $\langle n_{pe} \rangle$ decreases, respectively. So $60 \times 60 \times 120 \text{ cm}^3$ is the optimal size for water.

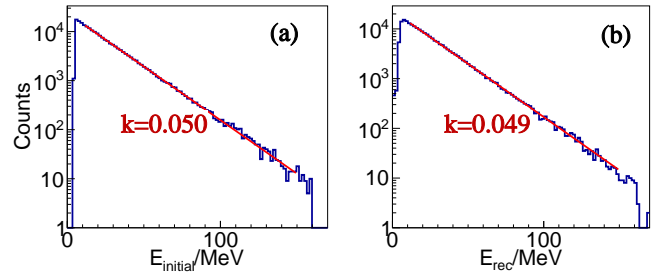


Figure 5: (Color online) The initial (a) and reconstructed (b) γ energy spectra in lead glass configuration.

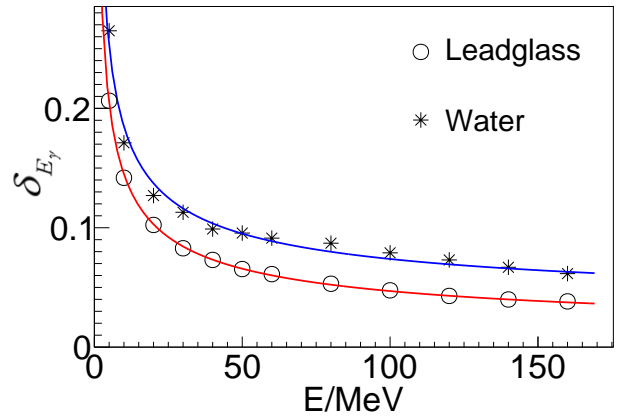


Figure 6: (Color online) Resolution prediction of the calorimeter of water and lead glass, respectively.

Given the good linear response for the water and lead glass Čerenkov calorimeter to the γ energy, as shown in Fig. 3 (b), one can reconstruct the γ energy from the signal height equivalent to the number of photoelectrons. To test the ability, we simulate the detector response for 10^5 γ events with the initial energy $E_{initial}$ in an exponential distribution. The slope of the input exponential distribution is set as -0.05 , as shown in Fig. 5 (a). The reconstructed energy (E_{rec}) is plotted in panel (b), with the slope parameter being fitted at -0.049 . It is shown that the Čerenkov calorimeter of lead glass measures the high-energy γ

in the range of 5-160MeV. Fig. 6 shows the resolution at various incident energies for lead glass and water configurations, respectively. The inherent resolution of $0.022 + 0.51/E_\gamma^{1/2}$ for water and $0.002+0.45/E_\gamma^{1/2}$ for lead glass are obtained by fitting the simulated data points. At high energies(above 100 MeV), the resolutions saturate at about 7.3% and 4.7%, respectively.

3.2. Direction reconstruction

As well known, there is a definite angle between Čerenkov photons and the charged particle[15] which is the basis for direction reconstruction. In fact, γ shower also partially retain this feature, Fig.7 shows the angle distribution between the Čerenkov radiation direction and the initial direction of electrons (γ rays) in water (lead glass) which was obtained by Geant4 simulation, the energy of electron and γ was sampled evenly from 5 to 160MeV in the simulation. The refractive index of lead glass and water are 1.7 and 1.3, so the cosine of their Čerenkov angle are $\cos \theta_c \approx 0.58$ and 0.77, respectively. According to Fig.7, although the e^+e^- pair production and Compton effect may cause scattering, the emission angle distribution of Čerenkov photons produced by the EM shower is still related to the initial direction of γ rays. This indicates that the direction of γ rays can be reconstructed by referring to the method of electron direction reconstruction used in large experiments such as Super-Kamiokande and Sudbury Neutrino Observatory(SNO)[26, 27]. It is found in our work that the Čerenkov photons experience scattering many times before reaching PMTs in water due to the overlength of the medium, smearing heavily the initial direction information, so we only reconstructed the γ rays direction in the lead glass configuration.

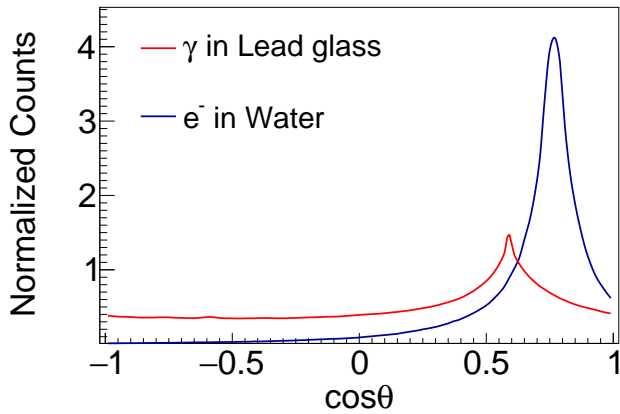


Figure 7: (Color online) Čerenkov photon direction distribution for electron incidence in water and γ ray incidence in lead glass, respectively.

3.2.1. Vertex reconstruction

For reconstructing the direction of electrons, it is usually assumed that electrons emit Čerenkov light from a fixed point. According to the angle distribution in Fig. 7, it can be assumed that the γ rays emit Čerenkov light from a fixed point with a specific Čerenkov angle, and hence the time of photon reaching the PMT can be expressed as [28, 29]

$$t_{\text{hit}} = \frac{|\vec{X}_{\text{pmt}} - \vec{X}_{\text{vtx}}|}{v} + t_0 \quad (3)$$

where t_0 represents the moment when the Čerenkov light is generated, t_{hit} represents the moment when the photon hits PMTs, v is the velocity of light in lead glass, \vec{X}_{pmt} and \vec{X}_{vtx} are the coordinate of the PMT and the vertex respectively. In our analysis, the optimal estimation of the vertex coordinates is obtained by minimizing the χ^2 of fitting the time distribution with formula (3), in which the t_0 and \vec{X}_{vtx} are fitting parameters. In each γ event, the timing on each PMT is extracted by linear fitting to the rising edge of waveform, where the crossing point of the linear fitting and zero baseline is taken as the timing signal of the PMTs[24]. The spatial coordinate of each firing PMT is used as \vec{X}_{pmt} . Since the reflector layer is set in the simulation, some Čerenkov photons will be reflected before hitting the PMTs and the timing signals will deviate from formula (3). So according to Fig. 2 (b), we only selected the PMTs with the hit time being less than 1.5 ns before the peak and 1 ns after the peak of the time distribution. We defined the coordinate for the center of lead glass as (0 cm, 0 cm, 0 cm). Fig. 8 shows the χ^2 distribution the vertex coordinate fitting for a 10 MeV γ ray incidence, indicating the optimal vertex coordinate at (1.29 cm, -1.11 cm, -6.34 cm).

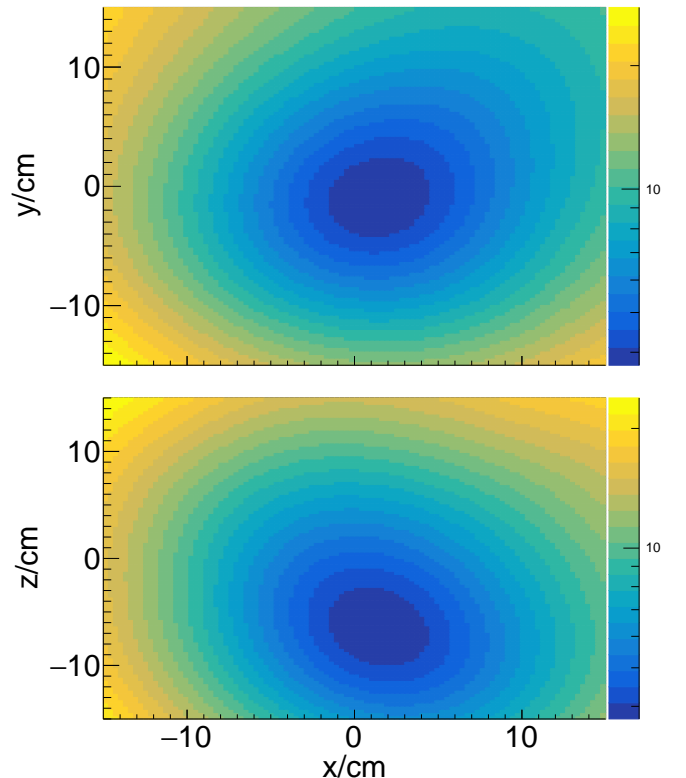


Figure 8: (Color online) The χ^2 distribution contour in the coordinate space of the vertex fitting.

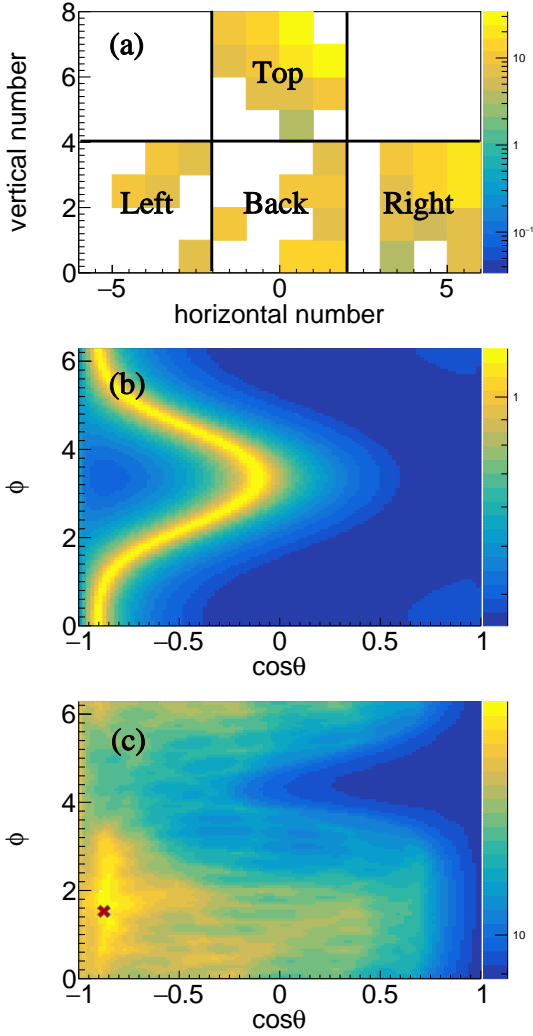


Figure 9: (Color online) Event display of Hough transformation. (a) is the position distribution of firing PMTs, there are four sides to place PMTs in lead glass configuration, top, left, right and back, (b) is the result of Hough transform for the marked 1st PMT on the back surface, (c) is the cumulative result of Hough transform for all firing PMTs in the time window. The cross indicates the optimized direction.

3.2.2. Hough transform

Hough transform[30, 31, 32] has been successfully applied to identify Čerenkov rings, which can map the vector space of the vertex-to-PMT direction to the vector space of the electron incident direction. An example of such application can be found in Super-Kamiokande[33]. Similarly, we can define the vector from the vertex of the γ ray to the firing PMT and the initial direction vector of the γ ray as \vec{V}_p and \vec{V}_γ respectively, and θ represents the angle between these two vectors. The probability distribution of θ is shown as the red line in Fig.7. The vector space of incident direction of γ ray was divided by 100×100 according to $(\cos \theta, \phi)$, and the weight of each cell can be expressed as

$$W_{ij} = \sum_1^k f(\cos \theta_{ijk}), \quad \cos \theta_{ijk} = \vec{V}_{\gamma ij} \cdot \vec{V}_{pk} \quad (4)$$

$\vec{V}_{\gamma ij}$ represents the central unit vector of the cell at row i and column j in the vector space of incident direction of γ ray, \vec{V}_{pk} represents the unit vector from the vertex pointing to the center of k^{th} firing PMT, and function f represents the Čerenkov angle distribution function of γ rays (the red line in Fig.7) in lead glass. Fig.9 shows the event display of Hough transform for the incident γ event in the direction of $(0.068, 0.063, -0.995)$. Fig.9(a) shows the hitting PMTs position distribution for this event, the color represents the signal amplitude in the corresponding PMT; Fig.9(b) shows the result of hough transform for the 1st PMT; Fig.9(c) shows the cumulative result of Hough transform for all the firing PMTs, the brightest point in Fig.9(c) represents the optimal estimate of the incident gamma direction. The optimal estimate is $(-0.077, 0.487, -0.87)$, and the deviation from the initial incidence direction is 26.9° for this event as an example.

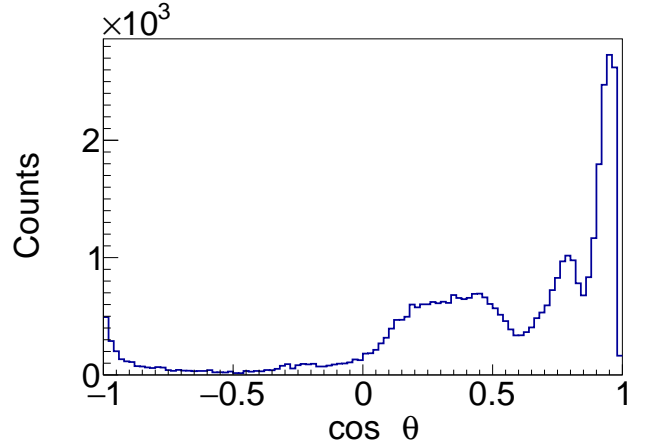


Figure 10: (Color online) The distribution of the angle between initial and reconstructed direction of γ rays

Fig.10 shows the distribution of $\cos \Delta\theta$, where $\Delta\theta$ is the angle between the reconstructed direction and the initial direction of γ rays hitting the front of lead glass uniformly from the target. It is shown that the peak of the cosine values is near $\cos \Delta\theta = 1$, indicating that the detector is able to reconstruct the direction of signal in the lead glass configuration. But the cosine distribution is broadened considerably due to the rough assumption that the γ rays emit Čerenkov light at a fixed point. In fact, according to the red line in Fig.7, most γ rays would generate Čerenkov light in a path whose length is comparable to the detector size, which is contribute to the bias in direction reconstruction. And the anti-symmetry of the locations of the PMTs also cause the bias.

3.2.3. Discrimination between γ and cosmic ray muon

In real beam experiment, only the γ rays from the reactions on the target are of interest. Since the direction of γ rays from the reaction target is different from cosmic ray, it provides a way to suppress the background. To test the ability of suppressing the cosmic-ray background, we generate γ rays with energy between 5 – 160 MeV to the front of detector and mix with uniform μ^- emissions from the top of detector. The μ^- energy

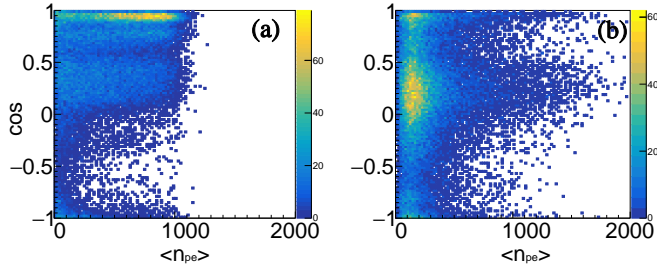


Figure 11: (Color online) Two-dimensional distribution of $\cos \Theta$ and $\langle n_{pe} \rangle$ for γ rays (a) from the reaction target and for cosmic ray muons (b).

E_μ (in GeV) and zenith angle θ_μ was sampled using the Gaisser formula [34]

$$\frac{dI}{dE_\mu d \cos \theta_\mu} = \frac{0.14}{E_\mu^{2.7}} \left[\frac{1}{1 + \frac{1.1E_\mu \cos \theta_\mu}{115}} + \frac{0.054}{1 + \frac{1.1E_\mu \cos \theta_\mu}{850}} \right] \quad (5)$$

Considering that the threshold for μ^- to produce Čerenkov in lead glass is 78 MeV, we set the sampling range of 80 – 1000 MeV. Here the physical quantity Θ denotes the angle between the reconstructed direction and the vector from reaction target to the fitted vertex vector. Fig.11 shows the two-dimensional distribution of $\cos \Theta$ and $\langle n_{pe} \rangle$ for γ rays from target (a) and for cosmic rays (b), respectively. Very different feature between the reaction γ rays and the cosmic ray muon background is evident. The $\cos \Theta$ of γ rays is concentrated above 0.5 and the $\langle n_{pe} \rangle$ is relatively evenly distributed between 0 and 1000, while the $\cos \Theta$ of μ^- is concentrated between 0 and 0.5 and the $\langle n_{pe} \rangle$ is concentrated around 200. Therefore, the directivity of the Čerenkov light provides a new dimension information for distinguishing the signal from the background.

4. Conclusion

In this work, we investigate the feasibility of using Čerenkov calorimeter to detect the bremsstrahlung γ rays from heavy ion reactions at Fermi energies. A full framework has been established to simulate the response and performance of the Čerenkov gamma calorimeter based on Geant 4 packages, including γ induced EM shower, Čerenkov photon generation and propagation, and the parameterization of PMT waveform. The optimal volume, linear response and energy resolution of the detector are obtained with water and lead glass being the sensitive medium, respectively. The inherent energy resolutions at $0.022 + 0.51/E_\gamma^{1/2}$ level for water and $0.002 + 0.45/E_\gamma^{1/2}$ for lead glass are predicted. It is demonstrated that the initial direction of γ rays can be reconstructed by using vertex fit and Hough transform method, showing the ability to distinguish the bremsstrahlung γ rays produced in the reactions from the cosmic ray muon background in real beam experiment. The detector will be built and applied shortly to measure high-energy γ rays produced in heavy ion reactions.

Acknowledgements

Supported by the Ministry of Science and Technology under Grant Nos. 2022YFE0103400 and 2020YFE0202001, by the National Natural Science Foundation of China under Grant Nos. 11961141004, 12205160 and by Tsinghua University Initiative Scientific Research Program.

References

- [1] M. A. Famiano, *et al.*, Neutron and Proton Transverse Emission Ratio Measurements and the Density Dependence of the Asymmetry Term of the Nuclear Equation of State. *Phys. Rev. Lett.* **97**, 052701 (2006). DOI: 10.1103/PhysRevLett.97.052701
- [2] Yongjia Wang, *et al.*, 3H/3He ratio as a probe of the nuclear symmetry energy at sub-saturation densities. *Eur. Phys. J. A* **51**, 37 (2015). DOI: 10.1140/epja/i2015-15037-8
- [3] Yongjia Wang, *et al.*, Application of microscopic transport model in the study of nuclear equation of state from heavy ion collisions at intermediate energies. *Front. Phys.* **15**, 44302 (2020). DOI: 10.1007/s11467-020-0964-6
- [4] Gao-Chan Yong, *et al.*, Neutron–proton bremsstrahlung from intermediate energy heavy-ion reactions as a probe of the nuclear symmetry energy. *Phys. Lett. B* **661**, 82–87(2008) DOI: 10.1016/j.physletb.2008.02.013
- [5] Bauer, G. F. Bertsch, *et al.*, Energetic photons from intermedium energy proton- and heavy-ion-induced reactions. *Phys. Rev. C* **34**, 2127(1986) DOI: 10.1103/PhysRevC.34.2127
- [6] Hui Xue, *et al.*, Neutron–proton bremsstrahlung as a possible probe of high-momentum component in nucleon momentum distribution. *Phys. Lett. B* **755**, 486-490(2016) DOI: 10.1016/j.physletb.2016.02.044
- [7] Antonov, A.N. *et al.*, Nucleon momentum and density distributions of nuclei. *Z Physik A* **297**, 257–260 (1980). DOI: 10.1007/BF01892806
- [8] Wen-Mei Guo, *et al* Imprints of high-momentum nucleons in nuclei on hard photons from heavy-ion collisions near the Fermi energy. *Phys. Rev. C* **104**, 034603(2021) DOI: 10.1103/PhysRevC.104.034603
- [9] F.H. Guan, *et al.*, A compact spectrometer for heavy ion experiments in the Fermi energy regime. *Nucl. Inst. Meth. A* **1011**, 165592 (2021). DOI: 10.1016/j.nima.2021.165592
- [10] F.H. Guan, *et al.*, Track recognition for the telescopes with silicon strip detectors. *Nucl. Inst. Meth. A* **1029**, 166461 (2022) DOI: 10.1016/j.nima.2022.166461
- [11] YuHao Qin, *et al.*, A CsI(Tl) hodoscope on CSHINE for Bremsstrahlung γ -rays in heavy ion reactions. *Nucl. Inst. Meth. A* **1053**, 168330 (2022) DOI: 10.1016/j.nima.2023.168330
- [12] Dong Guo, *et al.*, An FPGA-based trigger system for CSHINE. *Nucl. Sci. Tech.* **33**, 162(2022) DOI: 10.1007/s41365-022-01149-0
- [13] Yuhao Qin, *et al* Probing high-momentum component in nucleon momentum distribution by neutron-proton bremsstrahlung γ -rays in heavy ion reactions. arXiv:2307.10717v1 DOI: 10.48550/arXiv.2307.10717
- [14] Agostinelli S, Allison J, Amako K, *et al.*, Geant4—a simulation toolkit. *Nucl. Inst. Meth. A* **506**, 250-303(2022). DOI: 10.1016/S0168-9002(03)01368-8
- [15] Frank, I. M. and Tamm, I. E. Coherent visible radiation of fast electrons passing through matter. *Compt. Rend. Acad. Sci. URSS.* **14**, 109-114(1937). DOI: 10.3367/UfNr.0093.196710o.0388
- [16] J. Lundberg, *et al.*, Light tracking through ice and water—Scattering and absorption in heterogeneous media with PHOTONICS. *Nucl. Inst. Meth. A* **581**, 619-631(2007). DOI: 10.1016/j.nima.2007.07.143
- [17] M. Ackermann, *et al.*, Optical properties of deep glacial ice at the South Pole. *Journal of Geophysical Research Atmospheres.* **111**, D13203(2006) DOI: 10.1029/2005JD006687
- [18] Jenny Nilsson, *et al.*, Identifying key surface parameters for optical photon transport in GEANT4/GATE simulations. *Applied Radiation and Isotopes.* **103**, 15-24(2015). DOI: 10.1016/j.apradiso.2015.04.017
- [19] Rong-Sheng Lu, *et al.*, 3D surface topography from the specular lobe of scattered light. *Optics and Lasers in Engineering.* **45**, 1018-1027(2007). DOI: 10.1016/j.optlaseng.2007.04.008
- [20] Hecht, E. in *Optics*, ed. by Addison-Wesley(Boston, 1974), pp. 71-80 and pp. 244-246

- [21] A. Levin and C. Moisan., A more physical approach to model the surface treatment of scintillation counters and its implementation into DETECT. IEEE Nuclear Science Symposium. **2**, 702-706(1996) DOI: 10.1109/NSSMIC.1996.591410
- [22] Roncali, *et al.*, Simulation of light transport in scintillators based on 3D characterization of crystal surfaces. Physics in medicine and biology. **58**, 2185-2198(2013). DOI: 10.1088/0031-9155/58/7/2185
- [23] S. Riggi, *et al.*, GEANT4 simulation of plastic scintillator strips with embedded optical fibers for a prototype of tomographic system. Nucl. Inst. Meth. A **624**, 583-590(2010). DOI: 10.1016/j.nima.2010.10.012
- [24] YI Han, *et al.*, Prototype studies on the forward MWDC tracking array of the external target experiment at HIRFL-CSR. Chinese Physics C **38**, 126002(2014). DOI: 10.1088/1674-1137/38/12/126002
- [25] A. Bellerive, *et al.*, The Sudbury Neutrino Observatory. Nuclear Physics B **908**, 30-51(2016) 10.1016/j.nuclphysb.2016.04.035
- [26] B. Aharmim, *et al.*, Determination of the ν_e and total 8B solar neutrino fluxes using the Sudbury Neutrino Observatory Phase I data set. Phys. Rev. C **75**, 045505(2007). DOI: 10.1103/PhysRevC.75.045502
- [27] S. Fukuda, *et al.*, The Super-Kamiokande detector. Nucl. Inst. Meth. A **501**, 418-462(2003). DOI: 10.1016/S0168-9002(03)00425-X
- [28] J. P. Cravens, *et al.*, Solar neutrino measurements in Super-Kamiokande-II. Phys. Rev. D **78**, 032002 (2008). DOI: 10.1103/PhysRevD.78.032002
- [29] K. Abe, *et al.*, Solar neutrino results in Super-Kamiokande-III. Phys. Rev. D **83**, 052010(2011). DOI: 10.1103/PhysRevD.83.052010
- [30] T. Furuno, *et al.*, Performance test of the MAIKo active target. Nucl. Inst. Meth. A **908**, 215-224(2018). DOI: 10.1016/j.nima.2018.08.042
- [31] Magnus Lindström., Track reconstruction in the ATLAS detector using elastic arms. Nucl. Inst. Meth. A **357**, 129-149(1995). DOI: 10.1016/0168-9002(94)01544-9
- [32] Hough, P. V. C. in *Machine Analysis of Bubble Chamber Pictures*, ed. by Kowarski, L.(1959), pp. 554-558.
- [33] M. Shiozawa., Reconstruction algorithms in the Super-Kamiokande large water Cherenkov detector. Nucl. Inst. Meth. A **433**, 240-246(1999). DOI: 10.1016/S0168-9002(99)00359-9
- [34] Gaisser, T., *et al* in *Cosmic Rays and Particle Physics*, ed. by Press Syndicates of the University of Cambridge(1990), pp.69-81